

Prospects for probing dark matter particles and primordial black holes with the Square Kilometre Array using the 21 cm power spectrum at cosmic dawn

Meng-Lin Zhao,^{1,*} Yue Shao,^{1,2,†} Sai Wang,^{3,‡} and Xin Zhang^{1,4,5,§}

¹*Liaoning Key Laboratory of Cosmology and Astrophysics,*

College of Sciences, Northeastern University, Shenyang 110819, China

²*Department of Physics, Liaoning Normal University, Dalian 116029, China*

³*School of Physics, Hangzhou Normal University, Hangzhou 311121, China*

⁴*National Frontiers Science Center for Industrial Intelligence and Systems Optimization, Northeastern University, Shenyang 110819, China*

⁵*MOE Key Laboratory of Data Analytics and Optimization for Smart Industry, Northeastern University, Shenyang 110819, China*

Probing the nature of dark matter (DM) remains an outstanding problem in modern cosmology. The 21 cm signal, as a sensitive tracer of neutral hydrogen during cosmic dawn, provides a unique means to investigate DM nature during this critical epoch. Annihilation and decay of DM particles, as well as Hawking radiation of primordial black holes (PBHs), can modify the thermal and ionization histories of the early universe, leaving distinctive imprints on the 21 cm power spectrum. Therefore, the redshifted 21 cm power spectrum serves as a powerful tool to investigate such DM processes. In this work, we systematically assess the potential of the upcoming Square Kilometre Array (SKA) to constrain DM and PBH parameters using the 21 cm power spectrum. Assuming 10,000 hours of integration time, the SKA is projected to reach sensitivities of $\langle\sigma v\rangle \leq 10^{-28} \text{ cm}^3 \text{ s}^{-1}$ and $\tau \geq 10^{28}$ seconds, for 10 GeV DM particles. It can also probe PBHs with masses of 10^{16} g and abundances $f_{\text{PBH}} \leq 10^{-6}$. These results indicate that the SKA could place constraints on DM annihilation, decay, and PBH Hawking radiation that are up to two to three orders of magnitude stronger than current limits. Furthermore, the SKA is expected to exceed existing bounds on sub-GeV DM and to probe Hawking radiation from PBHs with masses above 10^{17} g, which are otherwise inaccessible by conventional cosmological probes. Overall, the SKA holds great promise for advancing our understanding of both DM particles and PBHs, potentially offering new insights into the fundamental nature of DM.

I. INTRODUCTION

Dark matter (DM) remains a major unsolved problem in modern cosmology. Astrophysical observations evidence that DM comprises more than 80% of the non-relativistic matter in the universe [1, 2]. Although numerous candidate models have been proposed to elucidate DM properties, the fundamental nature of DM remains unknown [3]. Particle DM candidates that interact weakly with ordinary matter, including weakly interacting massive particles (WIMPs), WIMP-like particles, and sub-GeV particles, can annihilate or decay into standard model particles [4, 5]. These standard model particles can subsequently generate distinctive signatures, which can be probed by instruments such as radio telescopes, neutrino detectors, and cosmic-ray observatories [6–8]. As non-particle DM candidates, primordial black holes (PBHs) can generate standard model particles including photons, electron-positron pairs, and neutrinos via the process of Hawking radiation [9]. Consequently, this process may also produce observable signatures [10–16]. However, no such evidence has been found. These null

detection results place stringent constraints on DM parameters (e.g., annihilation cross section, decay lifetime, and PBH mass and abundance), ruling out DM models incompatible with current observational data.

The 21 cm signal, particularly its power spectrum, provides a promising probe for DM [17–27]. Cosmic microwave background (CMB) observations place constraints on DM properties at recombination ($z \sim 1100$) [28–37], while cosmic rays and Lyman- α forest probe DM at low redshifts ($z \leq 6$) [38–61]. However, these approaches are ineffective at probing DM during the cosmic dawn. As a sensitive probe of neutral hydrogen, the 21 cm power spectrum captures the imprints of DM during this epoch via DM’s impact on the intergalactic medium (IGM), thereby bridging this observational gap. This occurs because DM particle annihilation, decay, and PBH Hawking radiation alter the thermal and ionization history of the IGM, thereby modifying the spin temperature of neutral hydrogen and affecting the brightness temperature of the 21 cm signal. The 21 cm power spectrum quantifies these brightness temperature fluctuations in three-dimensional space, thereby enabling the inference of DM properties.

To date, no 21 cm power spectrum signal has been detected, while the next-generation radio telescopes are expected to probe this signal for the first time. Existing radio telescopes, including the Murchison Widefield Array (MWA) [62, 63], the Low Frequency Array (LOFAR) [64, 65], and the Hydrogen Epoch of Reionization

* zhaoml@stumail.neu.edu.cn

† shaoyue0304@163.com

‡ Corresponding author; wangsai@hznu.edu.cn

§ Corresponding author; zhngxin@neu.edu.cn

Array (HERA) [66], have so far placed only upper limits on the 21 cm power spectrum. For example, MWA provided an upper limit of $(66.18 \text{ mK})^2$ at redshift $z = 7.1$ with scale $k = 0.19 h \text{ Mpc}^{-1}$ at the 95% confidence level [62, 63], while HERA reported an upper limit on the 21 cm power spectrum of $(30.76 \text{ mK})^2$ at the 95% confidence level at $z = 7.9$ with $k = 0.19 h \text{ Mpc}^{-1}$ [66]. The strictest upper limit arises from LOFAR, which is $(68.66 \text{ mK})^2$ at $z = 10.1$ with $k = 0.076 h \text{ Mpc}^{-1}$ at the 95% confidence level [64, 65]. As the next-generation flagship radio telescope, the Square Kilometre Array (SKA), with its high spectral resolution and wide field of view, is expected to enable the first precise measurements of the 21 cm power spectrum. The SKA construction has made progress, and its precursor array, SKA-AA0.5, has successfully obtained its first scientific image [67]. When operational, the SKA will constrain DM annihilation, decay, and PBH Hawking radiation via their imprints on the 21 cm power spectrum, potentially providing unprecedented constraints on DM properties, thus offering new insights into its fundamental nature.

In this work, we focus on the potential of the SKA to investigate DM. We first simulate the 21 cm power spectrum that incorporates the effects of DM particle annihilation, decay, and PBH Hawking radiation. We then utilize the Fisher information matrix to quantify the SKA's project sensitivity in constraining DM parameters. Finally, we propose and optimize observation strategies for the SKA to probe DM. This work is expected to provide new avenues for studying the nature of DM.

The structure of this paper is as follows. Section II discusses the physical mechanisms of DM energy injection into IGM. Section III shows the impact of energy injection on the 21 cm power spectrum. Section IV provides an introduction to the Fisher information matrix analysis. Section V quantifies the potential of the SKA for constraining the DM parameters. Section VI is the summary and discussion.

II. SCENARIOS OF EXOTIC ENERGY

In this section, we describe the scenarios of DM-induced exotic energy injected into IGM. Throughout this work, ρ_{DM} encodes information on the distribution of DM, indicating $\rho_{\text{DM}} = \rho_{\text{DM}}(z, \mathbf{x})$ with z and \mathbf{x} , respectively, being the redshift and the comoving position.

A. Annihilation and decay of DM particles

The exotic energy can be injected into IGM due to the annihilation and decay of DM particles, denoted by χ . In this work, we consider the annihilation channels of $\chi\chi \rightarrow \gamma\gamma$, $\chi\chi \rightarrow e^+e^-$, $\chi\chi \rightarrow b\bar{b}$, and the decay channels of $\chi \rightarrow \gamma\gamma$, $\chi \rightarrow e^+e^-$, $\chi \rightarrow b\bar{b}$. For a given channel, the primary particles can generate the secondary particles due to the hadronization process, which is simulated

using PYTHIA [68] and PPPC4DMID [69]. In the following, we focus on photons and electron-positron pairs, which are either primary or secondary or both, since the exotic energy is deposited into the IGM primarily via them [70–73].

In this work, we focus on the s -wave annihilation, which is characterized by zero relative orbital angular momentum, resulting in an approximately constant thermally-averaged annihilation cross-section. For this process, the energy injection rate per unit volume is given by

$$\left(\frac{dE}{dVdt}\right)_{\text{inj}} = f_{\text{ann}}^2 \rho_{\text{DM}}^2 c^2 \frac{\langle\sigma v\rangle}{m_\chi}, \quad (1)$$

where f_{ann} and m_χ stand for the fraction and mass of DM particles that can annihilate, ρ_{DM} the energy density of DM, c the speed of light, and $\langle\sigma v\rangle$ the thermally averaged annihilation cross section for the given annihilation channel.

For the decay of DM particles, we have the energy of photons and electron-positron pairs per unit volume per unit temporal interval as

$$\left(\frac{dE}{dVdt}\right)_{\text{inj}} = f_{\text{dec}} \rho_{\text{DM}} c^2 \frac{1}{\tau}, \quad (2)$$

where f_{dec} stands for the fraction of DM particles that can decay, and τ the lifetime of DM particles for the given decay channel.

Throughout this work, we take $f_{\text{ann}} = f_{\text{dec}} = 1$ for simplicity, but can quickly recover them if necessary.

B. Hawking radiation of PBHs

The exotic energy can also be injected into the IGM via the Hawking radiation of PBHs [9]. In this work, we focus on PBHs within the mass regime of $\sim 10^{15} - 10^{18} \text{ g}$. This mass range is of particular interest because PBHs within it could constitute a significant fraction of DM while evading existing constraints. PBHs in this mass range have not yet evaporated, and their Hawking radiation is potentially detectable, contributing to the exotic energy injection into the IGM. In this work, we consider the emission products in the form of photons and electron-positron pairs, since the exotic energy is deposited into the IGM primarily via these particles [24–26].

We have their energy per unit volume per unit temporal interval as

$$\begin{aligned} \left(\frac{dE}{dVdt}\right)_{\text{inj}} &= \int_0^{5 \text{ GeV}} \frac{d^2 N}{dEdt} \Big|_\gamma n_{\text{PBH}} E dE \\ &+ \int_{m_e c^2}^{5 \text{ GeV}} \frac{d^2 N}{dEdt} \Big|_e n_{\text{PBH}} (E - m_e c^2) dE \end{aligned} \quad (3)$$

where $d^2 N/(dEdt)$ stands for the particle spectrum given by BlackHawk [74], m_e the electron mass, and n_{PBH} the

number density of PBHs. Here, n_{PBH} is related to the PBH abundance, denoted by f_{PBH} , as

$$n_{\text{PBH}} = \frac{f_{\text{PBH}}\rho_{\text{DM}}}{M_{\text{PBH}}}, \quad (4)$$

where M_{PBH} stands for the PBH mass. It should be noted that for simplicity we have assumed a monochromatic mass function of PBHs, though the extended ones can be incorporated if necessary.

III. IMPRINTS ON THE 21 CM POWER SPECTRUM

In this section, following the conventions of Refs. [75–77], we demonstrate imprints of the injected exotic energy on the 21 cm brightness-temperature fluctuations at cosmic dawn. We simulate the 21 cm signal using a modified version of `21cmFAST` [78]. In this work, we modify the equations within `21cmFAST` for the gas temperature T_{K} , the ionization fraction x_{e} , and the Lyman- α coupling efficiency x_{α} to incorporate the effects of exotic energy injection from DM. The modifications, detailed in Section III B, account for the heating, ionization, and Lyman- α flux induced by exotic injection. We employ the `darkhistory` code [70] to compute the coefficients for exotic energy deposition through heating, ionization, and Lyman- α scattering, namely F_{heat} , F_{HI} , F_{He} , and F_{exc} , as described in Section III B.

A. 21 cm power spectrum

The differential brightness temperature of the 21 cm signal evaluated at the observer is defined by

$$\begin{aligned} \delta T_b(\nu, \mathbf{x}) &\simeq 23 x_{\text{HI}}(z, \mathbf{x}) \left(\frac{0.15}{\Omega_{\text{m}}}\right)^{\frac{1}{2}} \left(\frac{\Omega_{\text{b}} h^2}{0.02}\right) \left(\frac{1+z}{10}\right)^{\frac{1}{2}} \\ &\times \left[1 - \frac{T_{\text{CMB}}(z)}{T_{\text{S}}(z, \mathbf{x})}\right] \text{ mK}, \end{aligned} \quad (5)$$

where $\nu = \nu_{21}/(1+z)$ is the redshifted frequency of 21 cm photons, x_{HI} the neutral fraction of hydrogen, T_{CMB} the temperature of the CMB, T_{S} the spin temperature of neutral hydrogen, Ω_{m} (or Ω_{b}) the present-day energy-density fraction of non-relativistic (or baryonic) matter, and h the dimensionless Hubble constant. Here, T_{S} is explicitly given by

$$T_{\text{S}}^{-1} = \frac{T_{\text{CMB}}^{-1} + x_{\alpha} T_{\alpha}^{-1} + x_{\text{c}} T_{\text{K}}^{-1}}{1 + x_{\alpha} + x_{\text{c}}}, \quad (6)$$

where T_{α} stands for the color temperature of Lyman- α photons, T_{K} the kinetic temperature of the IGM gas, x_{α} the Lyman- α coupling coefficient, and x_{c} the collisional coupling coefficient. Due to resonant scattering, T_{α} is tightly coupled to T_{K} , namely $T_{\alpha} \simeq T_{\text{K}}$.

The observable is defined as follows. We first define the fractional perturbation to the differential 21 cm brightness temperature as

$$\delta_{21}(\nu, \mathbf{x}) = \frac{\delta T_b(\nu, \mathbf{x})}{\overline{\delta T_b}(\nu)} - 1, \quad (7)$$

where $\overline{\delta T_b}$ stands for the spatial average of δT_b . We further define the dimensionless power spectrum for δ_{21} as

$$\langle \tilde{\delta}_{21}(z, \mathbf{k}) \tilde{\delta}_{21}^*(z, \mathbf{k}') \rangle = (2\pi)^3 \delta(\mathbf{k} - \mathbf{k}') \frac{2\pi^2}{k^3} \Delta_{21}^2(z, k), \quad (8)$$

where $\tilde{\delta}_{21}(z, \mathbf{k})$ is the Fourier mode of $\delta_{21}(\nu, \mathbf{x})$ with ν being replaced with $z = \nu_{21}/\nu - 1$ and \mathbf{k} (or k) being the comoving wavevector (or wavenumber), $\langle \dots \rangle$ the ensemble average, and $\delta(\mathbf{k} - \mathbf{k}')$ the Dirac delta function. Following the conventions of Ref. [75], we define the 21 cm power spectrum in units of temperature as $\overline{\delta T_b}^2(z) \Delta_{21}^2(z, k)$, in which we have replaced ν with z once again. In the following, the above observable would be frequently referred to.

B. Imprints of the exotic energy

Once injected into IGM, the exotic energy can be deposited into IGM, thus altering the thermal and ionization histories of IGM. It can also contribute to the Lyman- α flux, altering the Lyman- α coupling coefficient. Therefore, we expect the injected exotic energy to leave imprints on the 21 cm power spectrum.

Due to energy deposition processes, the exotic energy can heat and ionize the IGM gas. The heating and ionizing rates per baryon, respectively, are given by

$$\epsilon_{\text{exo,heat}} = F_{\text{heat}}(z) \frac{1}{n_{\text{b}}} \left(\frac{dE}{dV dt}\right)_{\text{inj}}, \quad (9)$$

$$\begin{aligned} \Lambda_{\text{exo,ion}} &= F_{\text{HI}}(z) \frac{1}{n_{\text{b}}} \frac{n_{\text{H}}}{n_{\text{b}}} \frac{1}{E_{\text{ion}}^{\text{HI}}} \left(\frac{dE}{dV dt}\right)_{\text{inj}} \\ &+ F_{\text{He}}(z) \frac{1}{n_{\text{b}}} \frac{n_{\text{He}}}{n_{\text{b}}} \frac{1}{E_{\text{ion}}^{\text{He}}} \left(\frac{dE}{dV dt}\right)_{\text{inj}}. \end{aligned} \quad (10)$$

Here, we adopt the delayed energy deposition model that is integrated in `Darkhistory`. F_{heat} , F_{HI} , and F_{He} represent the energy deposition efficiencies via the processes of IGM heating, hydrogen ionization, and helium ionization, respectively. These deposition efficiencies are estimated by the `darkhistory`. n_{b} , n_{H} , and n_{He} denote the number densities of baryons, hydrogen, and helium, respectively. $E_{\text{ion}}^{\text{HI}}$ and $E_{\text{ion}}^{\text{He}}$ are the ionization energies of hydrogen and helium, respectively.

Considering both astrophysical processes and exotic energy, we have the heating and ionizing equations of

the IGM gas as

$$\frac{dT_K(z, \mathbf{x})}{dz} = \frac{2}{3k_B(1+x_e)} \frac{dt}{dz} (\epsilon_{\text{exo,heat}} + \epsilon_{\text{X,heat}} + \epsilon_{\text{IC,heat}}) + \frac{2T_K}{3n_b} \frac{dn_b}{dz} - \frac{T_K}{1+x_e} \frac{dx_e}{dz}, \quad (11)$$

$$\frac{dx_e(z, \mathbf{x})}{dz} = \frac{dt}{dz} (\Lambda_{\text{exo,ion}} + \Lambda_{\text{X,ion}} - \alpha_A C x_e^2 n_H). \quad (12)$$

Here, T_K and $x_e = 1 - x_{\text{HI}}$, respectively, represent the kinetic temperature and ionization fraction. k_B is the Boltzmann constant. t is the cosmic time. $\epsilon_{\text{X,heat}}$ and $\epsilon_{\text{IC,heat}}$, respectively, stand for the heating rates per baryon due to astrophysical X-rays and inverse-Compton scattering. $\Lambda_{\text{X,ion}}$ is the ionization rate due to astrophysical X-rays. α_A denotes the case-A recombination coefficient. C is the clumping factor. We have modified the corresponding equations in **21cmFAST**.

Due to the deposition, the exotic energy can also have a contribution to the Lyman- α flux, i.e.,

$$J_{\alpha,\text{exo}} = F_{\text{exc}}(z) \frac{1}{n_b} \frac{cn_b}{4\pi} \frac{1}{E_\alpha} \frac{1}{H(z)\nu_\alpha} \left(\frac{dE}{dVdt} \right)_{\text{inj}}. \quad (13)$$

Here, F_{exc} represents the energy deposition efficiency via the process of hydrogen excitation. It is also given by **darkhistory**. E_α and ν_α , respectively, denote the energy and frequency of Lyman- α photons. $H(z)$ is the Hubble parameter at z .

Taking into account Eq. (13), we modify the Lyman- α coupling coefficient to

$$x_\alpha = \frac{1.7 \times 10^{11}}{1+z} S_\alpha (J_{\alpha,\text{exo}} + J_{\alpha,\text{X}} + J_{\alpha,\star}). \quad (14)$$

Here, S_α denotes a quantum-mechanical correction factor. $J_{\alpha,\text{X}}$ and $J_{\alpha,\star}$, respectively, stand for the Lyman- α fluxes contributed by astrophysical X-rays and stellar emissions. We have also modified the corresponding equations in **21cmFAST**. In Fig. 1, we show the lightcone slices of our fiducial model and of a model with DM particle decay for comparison.

IV. FISHER INFORMATION MATRIX

To quantify the sensitivity of the SKA in probing DM particles and PBHs, we employ the Fisher information matrix. Assuming Gaussian posterior distributions for relevant parameters, the Fisher matrix for the 21 cm power spectrum is given by [75]

$$F_{ij} = \sum_l \sum_m \frac{N_z N_k}{\sigma_{\text{tot}}^2(z_l, k_m)} \frac{\partial [\overline{\delta T_b^2}(z_l) \Delta_{21}^2(z_l, k_m)]}{\partial \theta_i} \times \frac{\partial [\overline{\delta T_b^2}(z_l) \Delta_{21}^2(z_l, k_m)]}{\partial \theta_j}. \quad (15)$$

In this work, we discretize the 21 cm power spectrum into $N_k \times N_z$ independent bins, following Ref. [79]. N_k

and N_z represent the numbers of linearly discretized bins in k and z , respectively. The k range is from 0.2 to 0.9 Mpc^{-1} , and the z range is from 6 to 20. $\sigma_{\text{tot}}^2(z_l, k_m)$ is the total noise for the 21 cm power spectrum in the redshift bin z_l and wavenumber bin k_m . θ_i and θ_j represent the i -th and j -th parameter in the parameter set.

The total noise on the 21 cm power spectrum measurement arises from three key sources [80]

$$\sigma_{\text{tot}}^2 \equiv \left[0.2 \overline{\delta T_b^2} \Delta_{21}^2 \right]^2 + \sigma_{\text{poisson}}^2 + \sigma_{\text{ins}}^2, \quad (16)$$

where the first term represents a conservative 20% theoretical uncertainty in modeling the 21 cm signal [81], the second term quantifies the cosmic variance due to finite simulation volume, and the third term denotes instrumental noise dominated by the system temperature [80]. The instrumental noise is related to the square of system temperature, i.e., $\sigma_{\text{ins}} \propto T_{\text{sys}}^2$, while the system temperature can be estimated by [80]

$$T_{\text{sys}}(\nu) = 16.3 \times 10^6 \text{ K} \left(\frac{\nu}{2 \text{ MHz}} \right)^{-2.53}. \quad (17)$$

In this work, we adopt this system temperature in package **21cmSense** [80] to estimate the instrumental noise of SKA. We adopt stations in the central area of the SKA1-low (an array of 295 stations, where the diameter of each station is 35 m, distributed across a circular area with a diameter of 1.7 km), observing with a total bandwidth of 8 MHz and spectral resolution of 100 kHz, and a total integration time of 10,000 hours [82]. Marginalized uncertainty for a specific parameter θ_i satisfies $\sigma_{\theta_i} \geq \sqrt{(F^{-1})_{ii}}$ [83]. This suggests that the Fisher matrix provides conservative lower bounds on parameter constraints. The 1σ uncertainty of the parameter θ_i is its standard deviation. Furthermore, the correlation between parameters θ_i and θ_j is quantified by the dimensionless correlation coefficient $R_{ij} = C_{ij} / \sqrt{C_{ii}C_{jj}}$, where the covariance matrix C_{ij} is the inverse of the Fisher matrix F_{ij} .

Our model incorporates two categories of independent parameters, which are astrophysical parameters and parameters for DM particles and PBHs. Astrophysical parameters follow the conventions of **21cmFAST**, including t_\star , a_\star , a_{esc} , $\log_{10} f_\star$, $\log_{10} f_{\text{esc}}$, and $\log_{10} L_X$, where t_\star is the dimensionless star formation timescale, a_\star represents the power-law index of stellar-to-halo mass ratio, a_{esc} represents the power-law index of UV photon escape fraction, $\log_{10} f_\star$ represents the stellar-to-halo mass ratio, $\log_{10} f_{\text{esc}}$ represents the UV escape fraction, and $\log_{10} L_X$ represents X-ray luminosity per star formation rate in unit of $\text{erg} \cdot \text{yr} \cdot \text{sec}^{-1} M_\odot^{-1}$, where M_\odot stands for the solar mass. The remaining parameters correspond to DM physics. $\langle \sigma v \rangle$ characterizes the annihilation cross section of DM particles, in units of $\text{cm}^3 \text{ s}^{-1}$. $\Gamma = \tau^{-1}$ represents the decay rate of DM particles, in units of s^{-1} . f_{PBH} signifies the abundance of PBHs. For the fiducial model in Fig. 2, the astrophysical parameters are set to $t_\star = 0.5$, $a_\star = 0.5$, $a_{\text{esc}} = -0.5$, $\log_{10} f_\star = -1.3$, $\log_{10} f_{\text{esc}} = -1.0$,

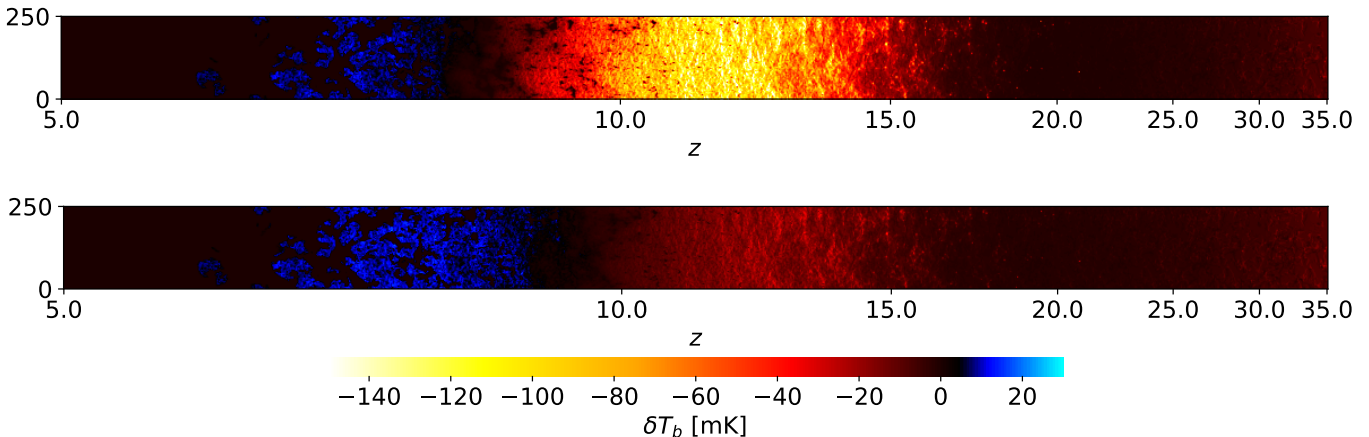


Figure 1. Lightcone slices of the differential brightness temperature in our $(250 \text{ Mpc})^3$ large simulation box. The fiducial model are shown on the upper panel. The bottom panel show the slice with DM particle annihilation through $\chi \rightarrow e^+e^-$ channel with $m_\chi = 10 \text{ GeV}$ and $\tau = 10^{27} \text{ s}$.

and $\log_{10} L_X = 40.0$, while the DM and PBH parameters, $\langle\sigma v\rangle$, Γ , and f_{PBH} are set to zero.

We demonstrate how the 21 cm power spectrum responds to exotic energy injections and present the SKA’s measurement errors on it, as shown in Fig. 2. The left panels display the redshift evolution of the 21 cm power spectrum at different scales, revealing peaks during cosmic dawn ($z \sim 10 - 15$) and the epoch of reionization ($z \sim 6 - 8$). The peak during cosmic dawn is dominated by the heating and ionizing effects of the IGM, rendering the amplitude of this peak highly sensitive to energy injection processes such as DM particle annihilation, decay, and PBH Hawking radiation. During cosmic dawn, exotic heating increases the IGM kinetic temperature, thereby suppressing the 21 cm power spectrum amplitude. Subsequently, after heating saturation, rising ionization causes the cosmic dawn peak to diminish. Conversely, the peak during the epoch of reionization is governed by the ionizing effect of the IGM. According to Ref. [84], an increased ionization fraction amplifies the power spectrum during reionization. This opposing response stems from distinct physical mechanisms, ionization reduces neutral hydrogen density during cosmic dawn, but enhances fluctuations in the ionized bubble during reionization. The right panels show the scale dependence of the 21 cm power spectrum at fixed redshifts. Exotic energy injections enhance the amplitude of the power spectrum at $z = 8.2$, but suppress it at $z = 10.6$, consistent with Ref. [84]. Crucially, near the redshift of the cosmic dawn peak, both the amplitude of the 21 cm power spectrum and the corresponding signal-to-noise ratio increase significantly. Consequently, cosmic dawn emerges as the optimal observational window for the SKA to probe DM.

V. DISCOVERING POTENTIAL OF SKA

In this section, we present the projected sensitivity of the SKA for probing DM particles and PBHs. We further compare this sensitivity with existing constraints from astrophysical probes.

A. Results for DM particles

The results of the Fisher information matrix analysis are summarized in Figs. 3–6. Figs. 3 and 5 display two representative corner plots that characterize parameter correlations and constraints, assuming a fixed DM particle mass of 100 MeV and an integration time of 10,000 hours. The 1σ and 2σ confidence intervals are represented by the dark and light shaded areas, respectively, while the solid curves depict the marginalized posterior distributions. Fiducial model parameters in these figures are consistent with those in Fig. 2. Complete corner plots are provided in Appendix A. Figs. 4 and 6 quantify the projected sensitivity at 1σ confidence level for SKA’s capability to probe DM and compare these results with existing constraints at 2σ confidence level from CMB observations [30], gamma ray measurements [45, 49–51, 55, 57, 58], electron-positron pair observations [48, 52, 53], and 21 cm global spectrum measurements [21].

Figs. 3 and 5 reveal mild correlations between the annihilation and decay parameters of DM particles and the astrophysical parameters. This result indicates a limited degeneracy between the DM-induced exotic energy injection and astrophysical effects on the 21 cm power spectrum. Specifically, $\langle\sigma v\rangle$ and τ show weak positive correlations with a_{esc} , a_\star and $\log_{10} f_\star$, mild negative correlations with t_\star , and negligible correlations with L_X and f_{esc} . These results demonstrate the feasibility of constraining

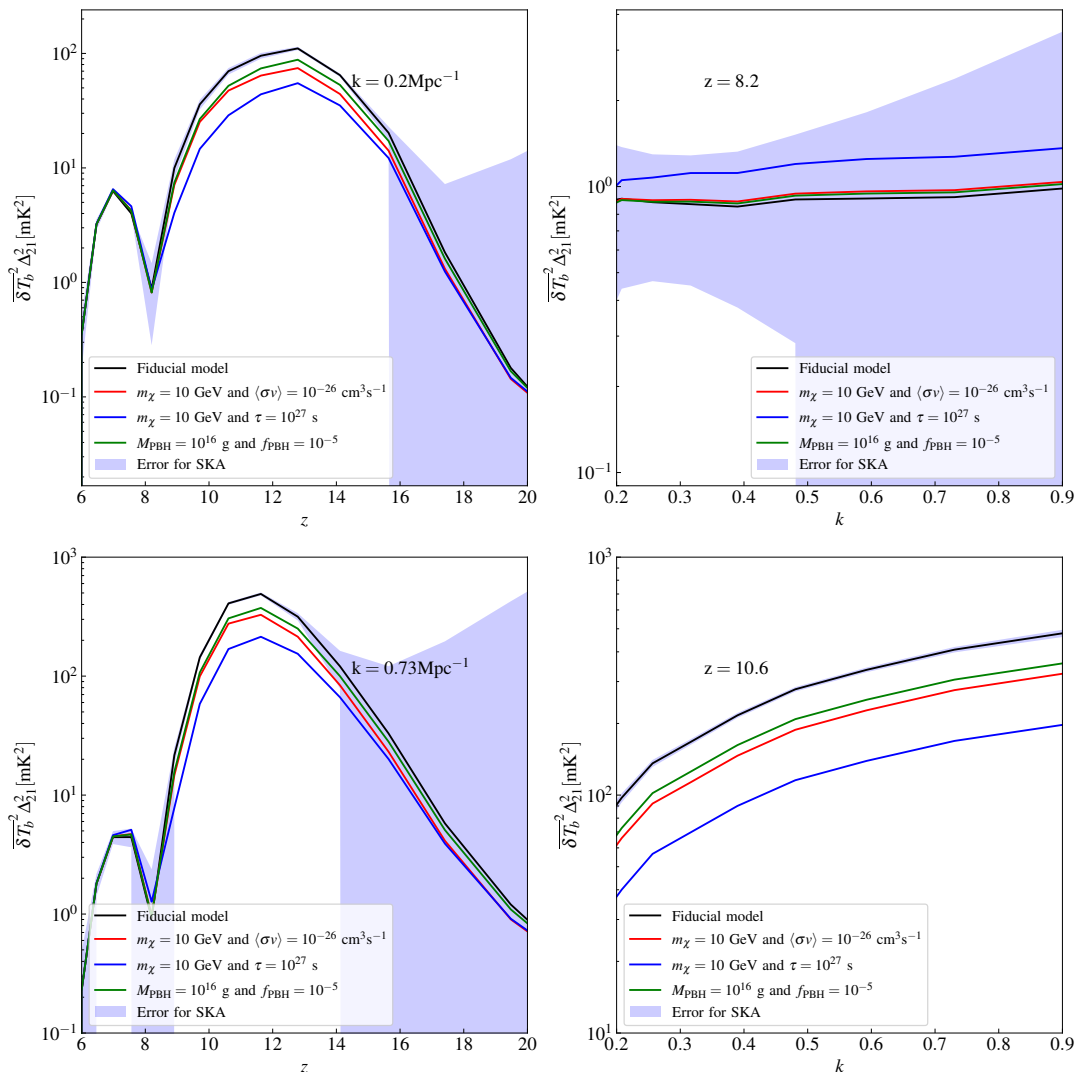


Figure 2. The 21 cm power spectrum under different energy injection scenarios. Left panels: The 21 cm power spectrum as a function of redshift z at fixed scales $k = 0.2 \text{ Mpc}^{-1}$ and $k = 0.73 \text{ Mpc}^{-1}$. Right panels: The 21 cm power spectrum as a function of the scale at redshift $z = 8.2$ and $z = 10.6$. In each panel, the instrumental noise is shown by the shaded region. Black curves show the 21 cm power spectrum of the fiducial model. Red curves show 21 cm power spectrum with DM particle annihilation through $\chi\chi \rightarrow e^+e^-$ channel with $m_\chi = 10 \text{ GeV}$ and $\langle\sigma v\rangle = 10^{-26} \text{ cm}^3 \text{ s}^{-1}$. Blue curves show 21 cm power spectrum with DM particle decay through $\chi \rightarrow e^+e^-$ channel with $m_\chi = 10 \text{ GeV}$ and $\tau = 10^{27} \text{ s}$. Green curves show 21 cm power spectrum with PBH Hawking radiation, with $M_{\text{PBH}} = 10^{16} \text{ g}$ and $f_{\text{PBH}} = 10^{-5}$.

DM parameters and extracting key properties, particularly the thermally-averaged annihilation cross section $\langle\sigma v\rangle$ and decay lifetime τ , using the 21 cm power spectrum. The weak degeneracies demonstrate that the 21 cm power spectrum can effectively constrain DM parameters independently of astrophysical uncertainties. This allows probing of fundamental DM properties, particularly $\langle\sigma v\rangle$ and τ , with minimized contamination from astrophysical processes.

Fig. 4 demonstrates SKA’s sensitivity to constrain DM annihilation via the $\chi\chi \rightarrow e^+e^-$ channel is superior to that for other channels such as $\chi\chi \rightarrow \gamma\gamma$ and $\chi\chi \rightarrow b\bar{b}$. Focusing on the optimal annihilation

channel $\chi\chi \rightarrow e^+e^-$ (upper panel), we find that utilizing the SKA, with 10,000 hours of integration time, the 21 cm power spectrum can achieve a sensitivity of $\langle\sigma v\rangle \leq 10^{-28} \text{ cm}^3 \text{ s}^{-1}$ for 10 GeV dark matter particles. This sensitivity surpasses the most stringent current constraints (gray curves), demonstrating SKA’s capacity to test existing limits in the near future. Furthermore, the SKA exhibits superior sensitivity to sub-GeV dark matter, a mass range where conventional probing experiments provide only weak constraints. While extended integration would improve sensitivity, practical implementation faces instrumental stability challenges [82].

The blue curve in Fig. 4 shows our previous result

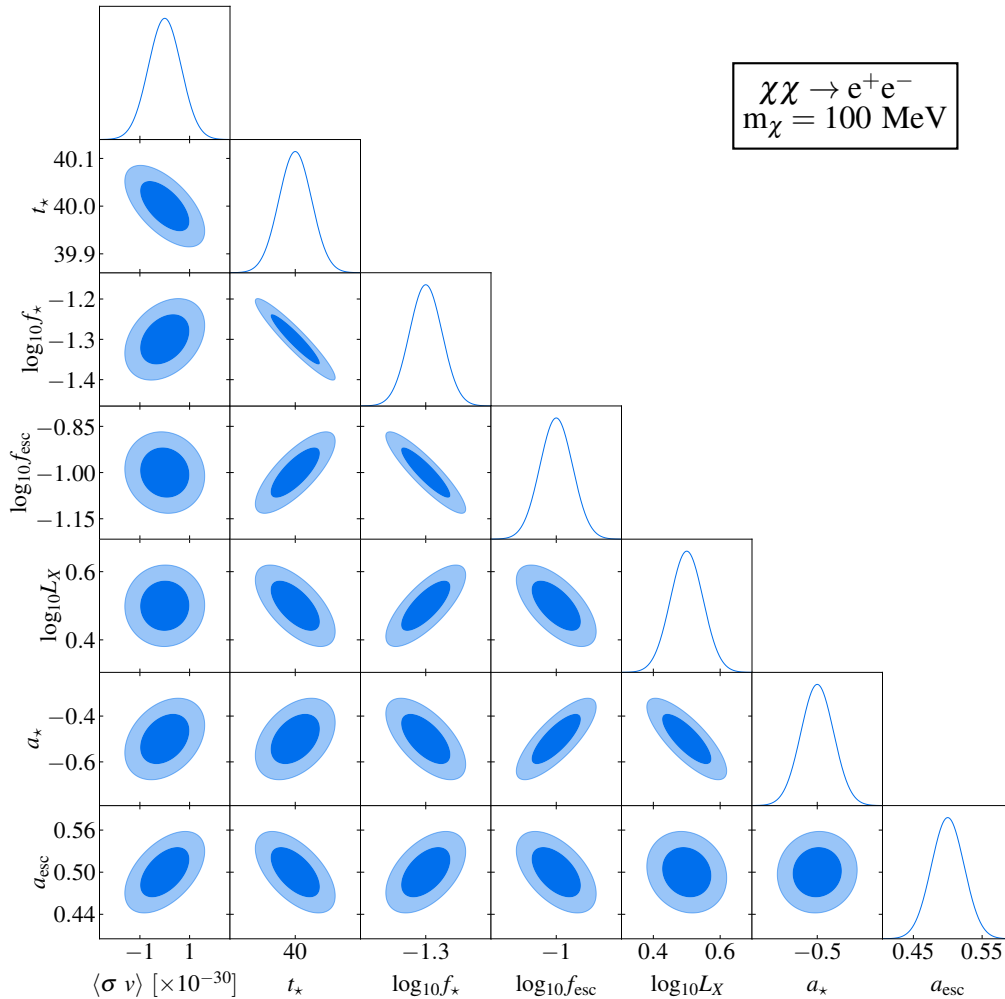


Figure 3. Fisher forecast for probing DM annihilation through the $\chi\chi \rightarrow e^+e^-$ channel using the 21 cm power spectrum by the SKA. 1σ and 2σ confidence intervals are represented by dark and light shaded areas, respectively, with solid curves indicating the marginalized posteriors. Fiducial model used is consistent with that shown in Fig. 2. The assumed DM particle mass is $m_\chi = 100 \text{ MeV}$, integrated over 10,000 hours.

based on the Hongmeng project, which assessed the capability of constraining DM annihilation parameters using the 21 cm global spectrum. In this work, we compare the results obtained by the SKA with those from Hongmeng. Our analysis reveals that the 21 cm power spectrum exhibits weaker correlations between DM parameters and astrophysical parameters than the 21 cm global spectrum. This reduced degeneracy enables the power spectrum to extract DM-induced signals more effectively. With the same integration time, the SKA achieves higher sensitivity than that implied by the results obtained by Hongmeng with the global spectrum, demonstrating its potential to probe DM annihilation signals beyond the reach of the global spectrum in the near future. Additionally, unlike the 21 cm global spectrum, the 21 cm power spectrum contains information on different scales.

Therefore, by probing the 21 cm power spectrum, the SKA is expected to provide insights into the properties of DM by measuring its effects on different scales, thus deepening our understanding of the DM nature.

Furthermore, a comparison between the power spectrum and the global spectrum from the SKA could provide more comprehensive insights. However, a detailed discussion of the Fisher matrix analysis and noise modeling for the global spectrum is beyond the scope of this paper. Therefore, we only present a qualitative analysis here, and defer a more thorough investigation to our upcoming work. Based on our previous work, constraints on DM derived from the global spectrum depend on its measurement error, which comprises two noise components: the foreground residual and the instrumental noise. In this work, the blue curve corresponds to a scenario with

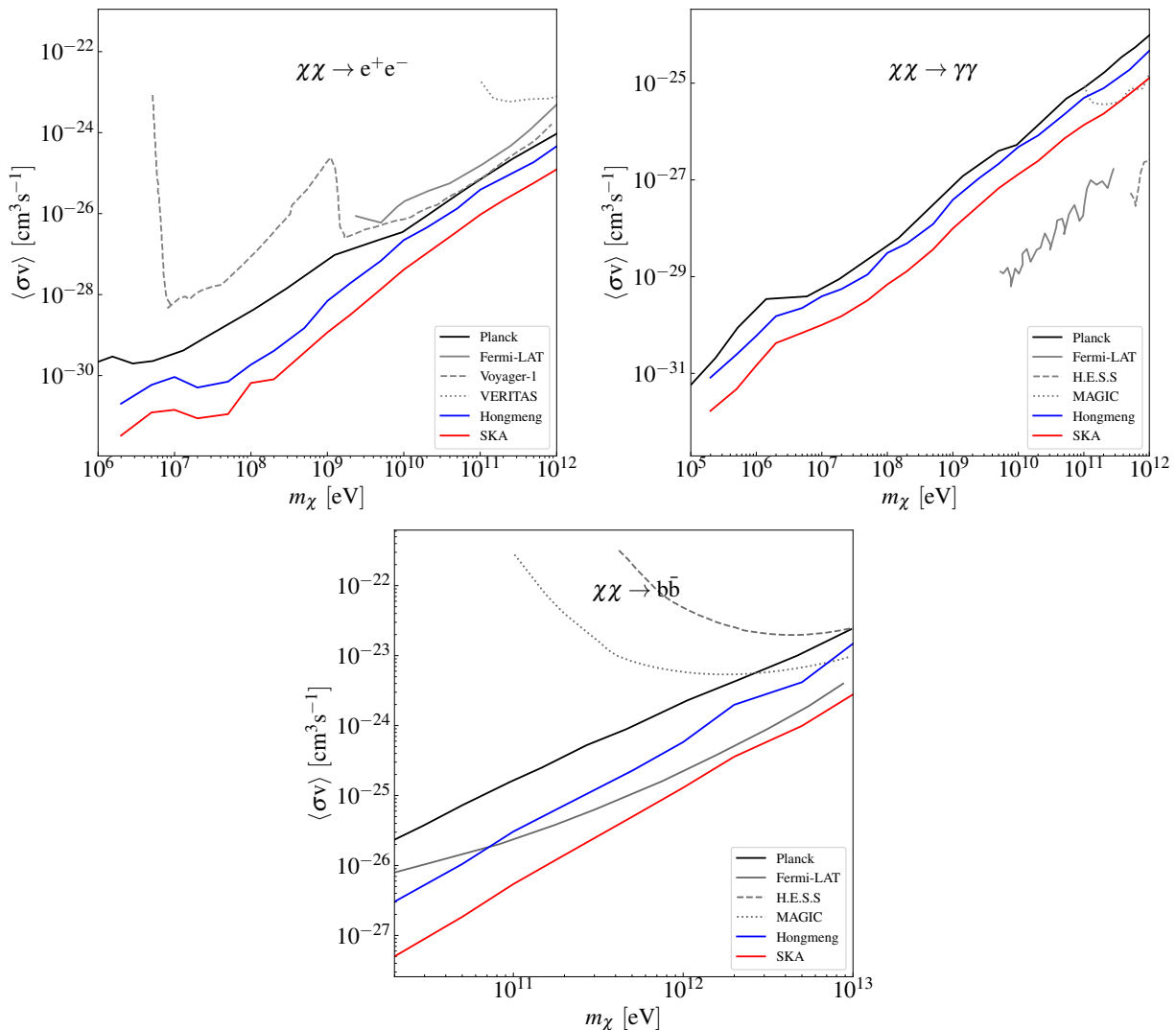


Figure 4. Prospective sensitivity of the SKA for probing the annihilation of DM particles through three channels. The 1σ confidence-level sensitivity of the SKA to the thermally averaged annihilation cross section of DM particles (mass range 10^6 - 10^{12} eV) are shown by the red curves. Existing 2σ upper limits from observations of CMB distortion (black curve) [30], gamma-ray observations (gray curves) [45, 49–51, 55, 57, 58], and electron-positron pairs (gray dashed curve) [48, 53] are included for comparison. Prospective sensitivity of the 21 cm global spectrum (blue curve) [21] is also included for comparison.

10,000 hours of observation time and a foreground residual level of 0.001. This configuration has already been examined in our previous work, in which the instrumental noise and foreground residual are comparable [21]. Changing the telescope only affects the instrumental noise, while the foreground noise remains unchanged. Assuming the same observational setup, i.e., 10,000 hours and 0.001 foreground residual, we can qualitatively analyze the measurement error of the SKA. Qualitatively, for a fixed integration time, the instrumental noise is approximately inversely proportional to the effective collecting area of the telescope. Given that the SKA has a much larger effective area than the spectrometer employed by the Hongmeng project, its instrumental noise is expected to be significantly lower for the same obser-

vation time. Thus, the instrumental noise of the SKA would be lower than the foreground residual, and the total noise would be dominated by the latter. Consequently, under the assumptions of 10,000 hours of integration and 0.001 foreground residual, observations with the SKA are not expected to yield better constraints than those from Hongmeng, which are represented by the blue curves. A more detailed quantitative analysis is beyond the aim of this paper. We plan to carry out a thorough and precise analysis in a forthcoming work.

Fig. 6 indicates that the SKA has superior sensitivity in constraining DM decay via the $\chi \rightarrow e^+e^-$ channel, compared to alternative channels such as $\chi \rightarrow \gamma\gamma$ and $\chi \rightarrow b\bar{b}$. Focusing on the optimal decay channel $\chi \rightarrow e^+e^-$ (upper panel), and assuming an inte-

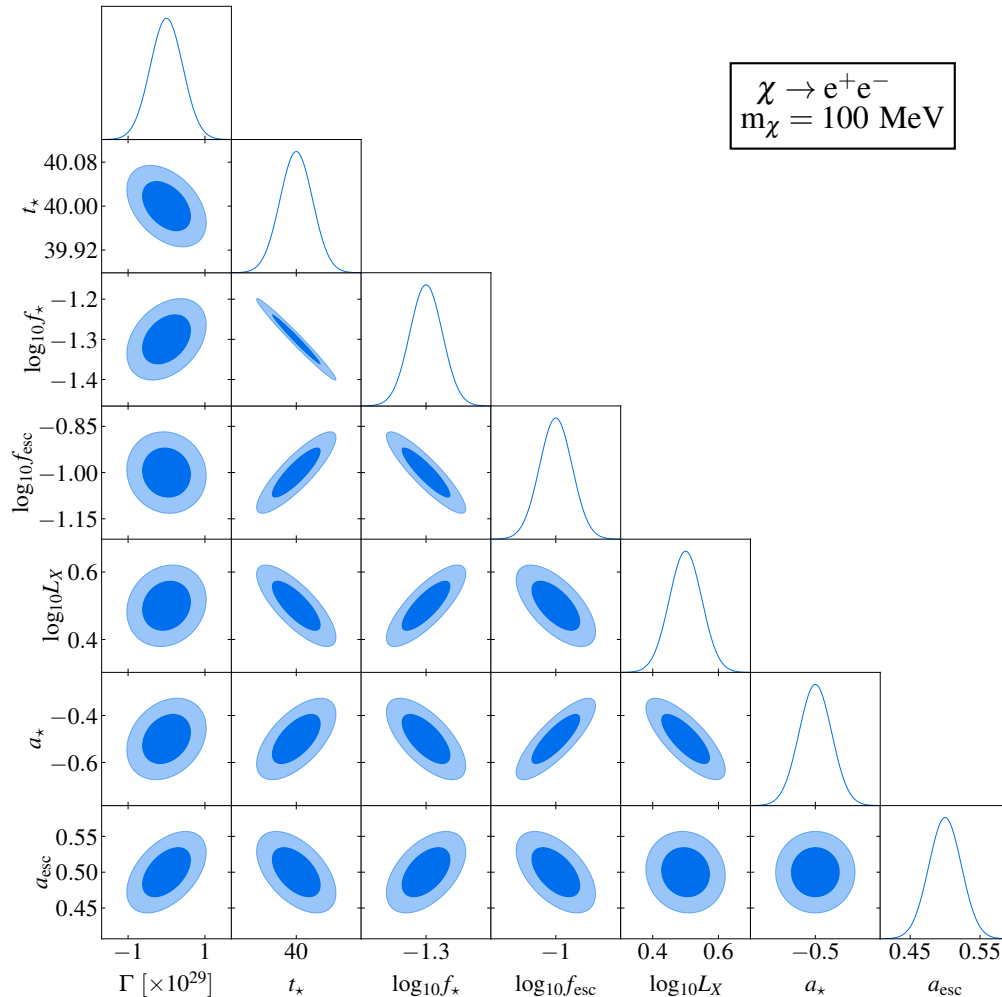


Figure 5. Fisher forecast for probing DM decay through the $\chi \rightarrow e^+e^-$ channel using the 21 cm power spectrum by the SKA. 1σ and 2σ confidence intervals are represented by dark and light shaded areas, respectively, with solid curves indicating the marginalized posteriors. Fiducial model used is consistent with that shown in Fig. 2. The assumed DM particle mass is $m_\chi = 100$ MeV, integrated over 10,000 hours.

gration time of 10,000 hours, the SKA is projected to improve constraints on the DM particle decay lifetime by two orders of magnitude, surpassing current experimental bounds (gray curves). This result demonstrates SKA’s potential to test existing DM decay models in the near future. While increasing the integration time would further improve sensitivity, practical implementation beyond 10,000 hours may require addressing instrumental stability limitations [82]. Notably, through 21 cm power spectrum measurements, the SKA achieves superior sensitivity to sub-GeV DM, a parameter space weakly constrained by current methods.

The blue curve in Fig. 6 represents our previous work, which explored the potential to probe DM decay using the 21 cm global spectrum from the Hongmeng Project. We perform a comparative analysis of DM decay con-

straints derived from the 21 cm power spectrum and the 21 cm global spectrum. Our analysis reveals less degeneracy between DM decay parameters and astrophysical parameters in the power spectrum compared with the global spectrum. This reduced degeneracy enables the power spectrum to more effectively extract DM-induced signatures. With the same integration time, the 21 cm power spectrum achieves a sensitivity one order of magnitude better than 21 cm global spectrum. This result demonstrates that the SKA will impose tighter constraints on DM decay parameter than those achieved with the 21 cm global spectrum. Furthermore, unlike the global spectrum, the 21 cm power spectrum encodes information across multiple spatial scales, enabling the probing of DM properties at different scales and deepening our understanding of DM’s fundamental nature.

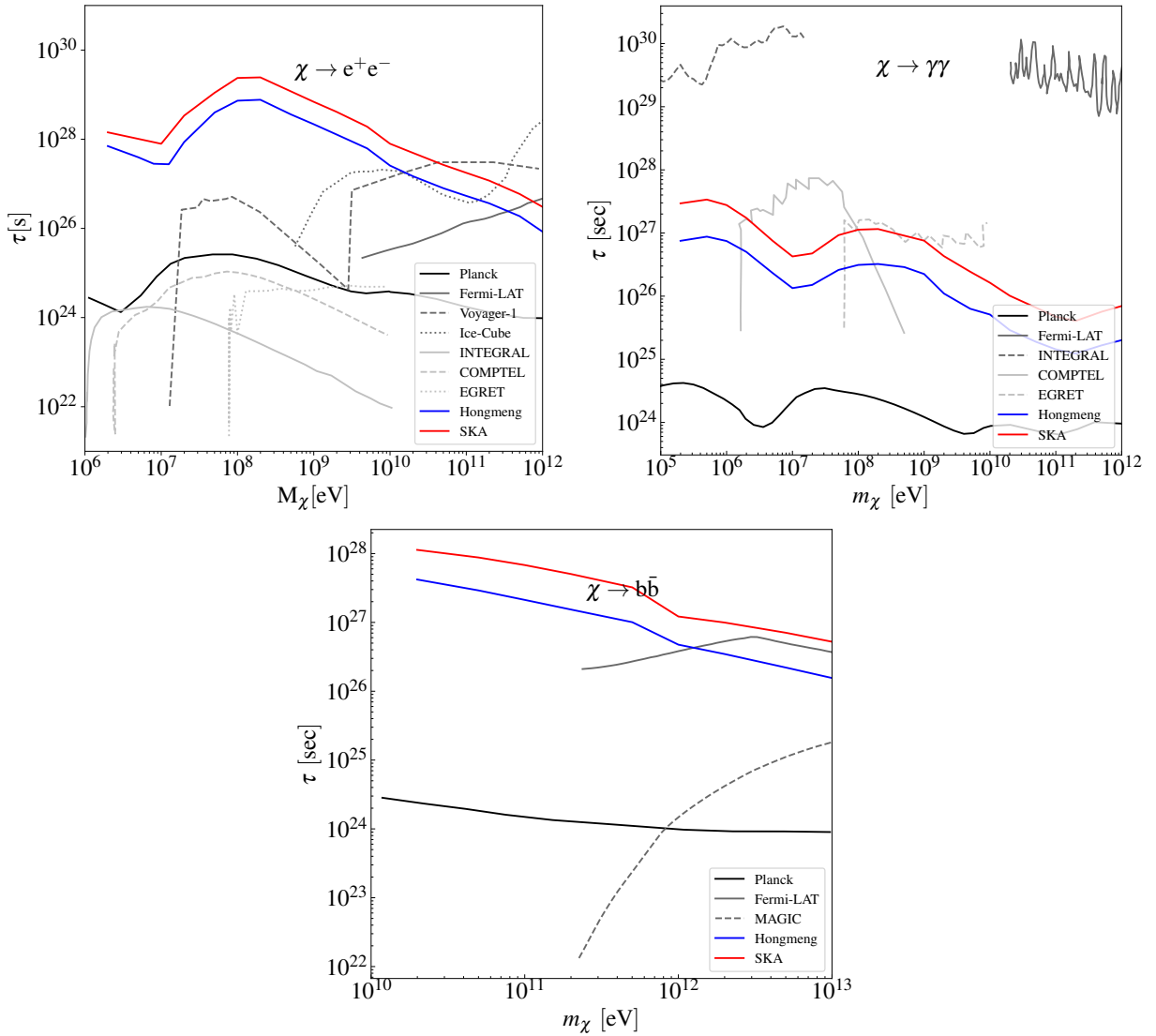


Figure 6. Prospective sensitivity of the SKA for probing the decay of DM particles through three channels. The 1σ confidence-level sensitivity of the SKA project to the decay lifetime of DM particles (mass range 10^6 - 10^{12} eV) are shown by the red curves. Existing 2σ upper limits from observations of CMB distortion (black curve) [29, 33], extragalactic photons (gray curves) [41–43, 45, 53, 56, 60], and electron-positron pairs (gray dashed curve) [48, 53] are included for comparison. Prospective sensitivity of the 21 cm global spectrum (blue curve) is also taken into consideration [21].

B. Results for PBHs

Figs. 7 and 8 summarize the results of our parameter estimation based on Fisher matrix analysis. Fig. 7 shows the correlations and constraints of model parameters for a 10^{16} g PBH with an integration time of 10,000 hours. Shaded regions represent the 1σ (dark) and 2σ (light) confidence regions. Corresponding one-dimensional marginalized posterior distributions are shown as solid curves. Fiducial model parameters are consistent with those in Fig. 2. Fig. 8 quantifies the SKA’s sensitivity to Hawking radiation for PBHs with mass ranging from 10^{15} g to 10^{18} g, assuming a fixed integration time of 10,000 hours, at the 1σ confidence level.

This sensitivity is compared with existing 2σ exclusion bounds from observations of the diffuse neutrino background [46], CMB anisotropy [31, 32, 34], gamma ray measurements [54], electron-positron pair measurements [47, 53], and 21 cm global signals [21].

Fig. 7 reveals weak correlations between the PBH abundance f_{PBH} and key astrophysical parameters. This result suggests weak degeneracies between the exotic energy injection from the PBH Hawking radiation and astrophysical effects on the 21 cm power spectrum. Specifically, f_{PBH} exhibits weak positive correlations with a_{esc} , a_* , and $\log_{10} f_*$, and a negative correlation with t_* . In contrast, f_{PBH} shows no significant correlations with L_X and $\log_{10} f_{\text{esc}}$. These weak degeneracies enable the 21

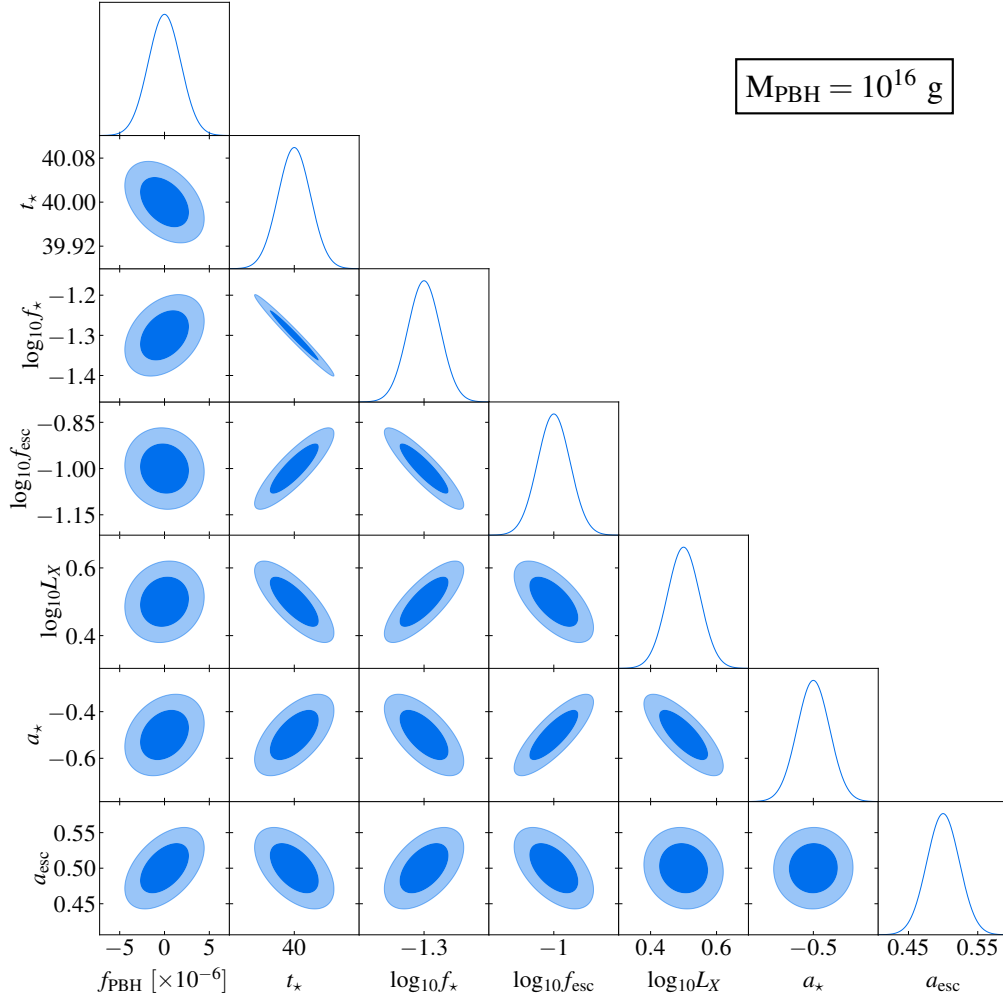


Figure 7. Fisher forecast for probing PBH Hawking radiation using the 21 cm power spectrum by the SKA. Dark and light shaded regions correspond to contours at 1σ and 2σ confidence intervals, respectively. Solid curves represent the marginalized posteriors of the model parameters. Fiducial model used is consistent with that shown in Fig. 2. The mass of PBH is assumed to be $M_{\text{PBH}} = 10^{16}$ g, with an integration duration of 10,000 hours.

cm power spectrum to constrain PBH properties while minimizing contamination from astrophysical uncertainties. This result allows the probing of fundamental PBH properties, particularly the abundance f_{PBH} .

Based on the results in Fig. 8, we demonstrate that the 21 cm power spectrum measured by the SKA achieves a sensitivity to $f_{\text{PBH}} \simeq 10^{-10}$ for PBHs with masses of 10^{15} g, assuming an integration time of 10,000 hours. This result surpasses constraints from existing observations (gray curves) by up to 3–4 orders of magnitude, indicating that the SKA can test these results in the near future. Moreover, the SKA extends sensitivity to higher-mass PBHs compared with current experiments, particularly probing the unexplored mass range above 10^{17} g. While extended integration would improve sensitivity, practical operation beyond 10,000 hours may be

limited by instrumental stability constraints [82].

Our prior analysis using Hongmeng’s 21 cm global spectrum also established PBH abundance constraints. Such results are presented by the blue curve in Fig. 8. In this work, we compare the constraints on PBHs derived from the 21 cm power spectrum with those obtained from the 21 cm global spectrum. Our result indicates a weaker coupling of PBH abundance and astrophysical parameters in the 21 cm power spectrum than that in the global spectrum. With the same integration time, the 21 cm power spectrum using the SKA reaches a sensitivity nearly an order of magnitude higher than that achieved by the 21 cm global spectrum with Hongmeng. This result suggests that, in the near future, the SKA is expected to place tighter constraints on PBH abundance than those obtained from the 21 cm global spectrum, thus

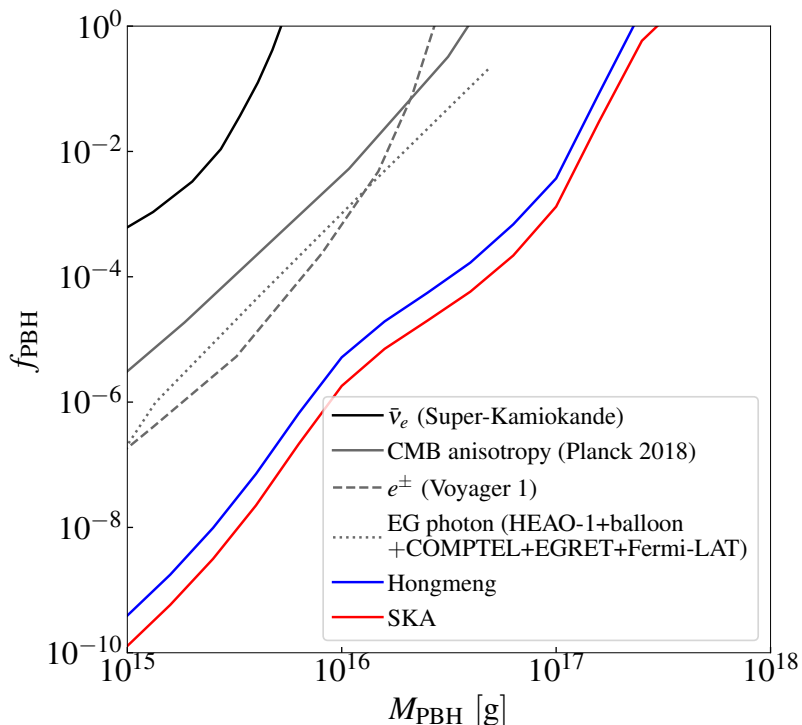


Figure 8. Prospective sensitivity of the SKA for probing the PBHs. The 1σ confidence-level sensitivity of the SKA project to measure the abundance of PBHs within the mass range of $10^{15} - 10^{18}$ g is shown by the red curve. For comparison, we show the existing upper limits at 2σ confidence level from observations of the diffusion neutrino background (black curve) [46], CMB anisotropies (gray solid curve) [31, 32, 34], extra-galactic photons (gray dotted curve) [54], and electron-positron pairs (gray dashed curve) [47]. Prospective sensitivity of the 21 cm global signal (blue curve) is also taken into consideration.

allowing us to probe PBHs with unprecedented precision.

VI. SUMMARY

In this work, we systematically assess the prospects for the SKA to probe DM particle annihilation, decay, and PBH Hawking radiation via the 21 cm power spectrum during cosmic dawn. Exotic energy from these DM processes can deposit into IGM, thereby heating and ionizing the IGM, significantly suppressing the 21 cm power spectrum. Utilizing Fisher matrix analysis, we quantify SKA’s sensitivity to the relevant parameters, specifically the annihilation cross section ($\langle\sigma v\rangle$), decay lifetime (τ), and PBH abundance (f_{PBH}). Our results demonstrate that, with its designed observational capabilities, the SKA is uniquely positioned to place breakthrough constraints on these parameters.

The SKA demonstrates great observational capability in probing DM particle annihilation and decay. Specifically, for DM annihilation and decay via channels producing electron-positron pairs, the SKA achieves optimal sensitivity for extracting DM signals using the 21 cm power spectrum during cosmic dawn. With 10,000 hours of integration time, the SKA is projected to reach sensitivities of $\langle\sigma v\rangle \leq 10^{-28} \text{ cm}^3 \text{ s}^{-1}$ and $\tau \geq 10^{28} \text{ s}$ for

10 GeV DM particles, surpassing existing astrophysical constraints by approximately 2 – 3 orders of magnitude. Moreover, it provides tighter constraints than current experimental limits on sub-GeV DM particles, deepening our understanding of DM properties.

For PBH Hawking radiation, the SKA can constrain the PBH abundance to $f_{\text{PBH}} \leq 10^{-6}$ for PBHs with masses of 10^{16} g and an integration time of 10,000 hours, representing a three-order-of-magnitude improvement over existing limits. Crucially, the SKA can probe more massive PBHs ($\geq 10^{17}$ g), which are currently undetectable by other probes, thereby opening a new window to test PBHs as DM candidates.

In summary, our analysis demonstrates that, during the cosmic dawn, the SKA can effectively probe DM annihilation, decay, and PBH Hawking radiation through 21 cm power spectrum measurements with 10,000 hours of integration time. The sensitivity of the SKA is fundamentally limited by instrumental noise, which decreases with increasing integration time. However, while insufficient integration time degrades detection sensitivity, significantly extending integration time introduces practical challenges in maintaining instrumental stability, a systematic consideration beyond the scope of this study.

It is noteworthy that in this work, we have not considered the scenario in which DM particle annihilation,

decay, and Hawking radiation from PBHs coexist. However, this represents an important scenario, which may provide valuable insights into the nature of DM. Methods such as the Fisher information matrix may help break the degeneracies among these mixed DM processes, but the relevant discussions are more complex and beyond the scope of this work. We anticipate conducting a more detailed investigation in our future work.

Furthermore, alternative methods such as the bispectrum, scattering transforms, and Minkowski functionals are also expected to provide additional constraining capability. For example, the bispectrum captures higher-order statistic information, i.e., the non-Gaussianity that is generally absent in the analysis of power spectrum [85–87]. However, this method is computationally more complex than the power spectrum due to the necessity to compute the three-point correlation function. Similarly, scattering transforms provide rich, high-order descriptions of signal morphology but require substantial computational resources to compute all scattering paths [88–90]. In contrast, Minkowski functionals are computationally efficient compared to the power spectrum, yet they offer limited scale-dependent information and are less sensitive to anisotropy [91]. Therefore, the power spectrum remains a relatively more cost-efficient approach compared with these methods. Nevertheless, since each method has its own advantages and limitations, a combined approach may yield particularly valuable insights. We are thus preparing a new work that incorporates such methods.

Looking beyond cosmic dawn, investigating the nature of DM during the dark ages ($z \gtrsim 30$) represents a frontier in cosmology. While recently the James Webb Space Telescope (JWST) has detected high-redshift galaxies [92], the dark ages remain observationally unexplored. As galaxies have not yet formed during this epoch, 21 cm signal provides the only radio probe for the dark ages. Crucially, unlike the 21 cm signal in cosmic dawn, the 21 cm signal in the dark ages is pristine, which is unaffected by astrophysical heating and ionization. Therefore, targeting the dark ages with next-generation radio telescopes like the SKA and the Hongmeng offers an effective pathway to probe fundamental physics of DM. Consequently, observations of dark ages circumvent the degeneracies between DM physics and astrophysics at lower redshift, enabling stringent constraints on the parameters of DM. In summary, 21 cm cosmology holds exceptional promise as a uniquely powerful probe for unveiling the physics of the early universe and the fundamental nature of DM.

Appendix A: Results of Fisher matrix analysis

Remaining results of Fisher matrix forecasts are shown in Figs. 9–12. Figs. 9 and 10 present the Fisher information matrix analysis results of DM particle annihilation through channels producing photon pairs and bottom-anti-bottom quark pairs. The dark and light shaded re-

gions correspond to 1σ and 2σ confidence level contours, respectively. The solid curves represent the marginalized posterior distributions of relevant parameters. The Fiducial parameter values are consistent with those in Fig. 2. For annihilation via the photon-pair channel, the DM particle mass is 10 MeV. For the bottom-anti-bottom quark pair channel, it is 10 GeV. Similarly, Figs. 11 and 12 present the Fisher matrix analysis results for DM particle decay through the same channels. The configuration settings are identical to those used in Figs. 9 and 10.

ACKNOWLEDGMENTS

We are grateful to Kazunori Kohri, Yichao Li, and Xukun Zhang for their valuable contributions to the discussion. This work is supported by the National SKA Program of China (Grant Nos. 2022SKA0110200, 2022SKA0110203), the National Key R&D Program of China (Grant No. 2023YFC2206403), the National Natural Science Foundation of China (Grant Nos. 12175243, 12473001, and 12533001), the China Manned Space Program (Grant No. CMS-CSST-2025-A02), and the National 111 Project (Grant No. B16009).

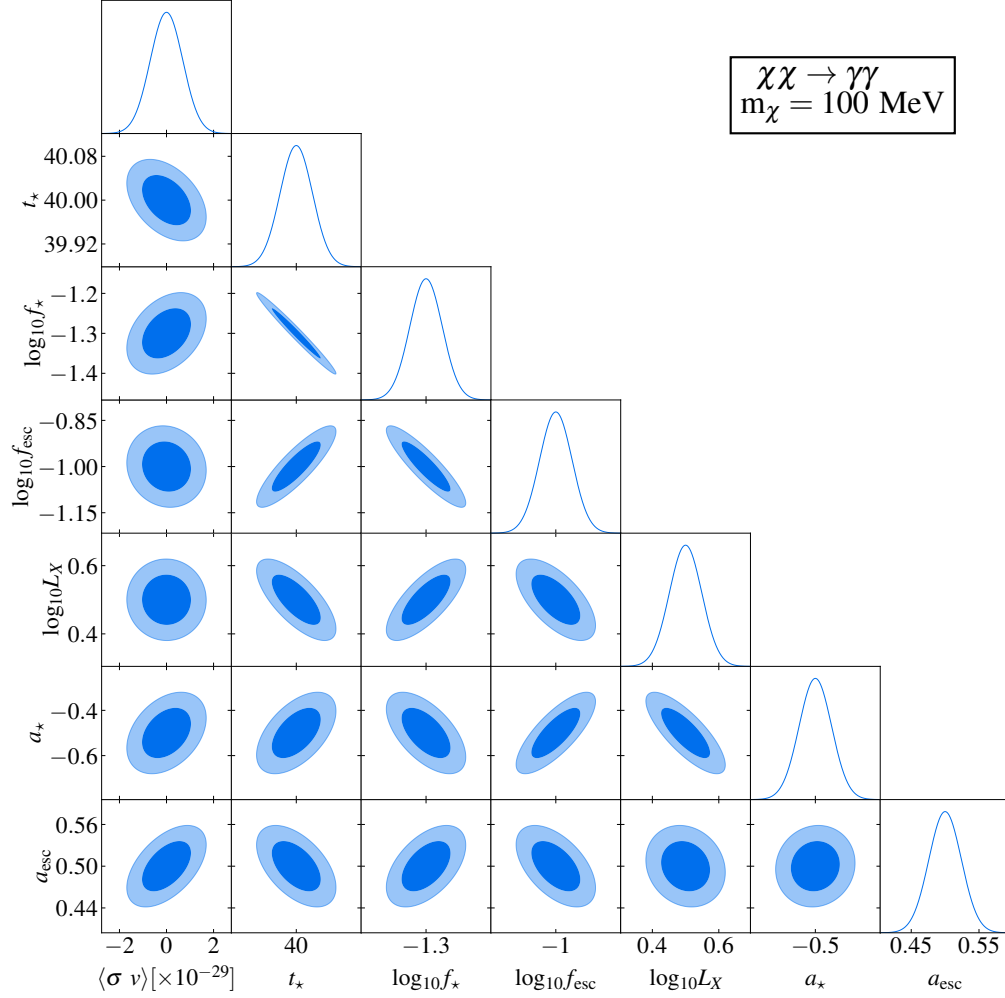


Figure 9. Fisher forecast for probing DM annihilation through the $\chi\chi \rightarrow \gamma\gamma$ channel using 21 cm power spectrum by the SKA. 1σ and 2σ confidence intervals are represented by dark and light shaded areas, respectively, with solid curves indicating the marginalized posteriors. Fiducial model used is consistent with that shown in Fig. 2. The assumed DM particle mass is $m_\chi = 100$ MeV, integrated over 10,000 hours.

-
- [1] PARTICLE DATA GROUP collaboration, *Review of particle physics*, *Phys. Rev. D* **110** (2024) 030001.
- [2] V.A. Rubakov, *Cosmology and dark matter*, *CERN Yellow Rep. School Proc.* **5** (2022) 129 [1912.04727].
- [3] G. Bertone and D. Hooper, *History of dark matter*, *Rev. Mod. Phys.* **90** (2018) 045002 [1605.04909].
- [4] H. Liu, *Dark Matter Energy Deposition and Production from the Table-Top to the Cosmos*, Ph.D. thesis, MIT, 2019. 1907.04324.
- [5] X.-L. Chen and M. Kamionkowski, *Particle decays during the cosmic dark ages*, *Phys. Rev. D* **70** (2004) 043502 [astro-ph/0310473].
- [6] C.R. Thorpe-Morgan, *Astrophysical Frontiers: The Indirect Detection of Dark Matter & the Analysis of Gamma-ray Binary Systems*, Ph.D. thesis, Universität Tübingen, Tübingen U., 10, 2024. 10.15496/publikation-99791.
- [7] J.M. Gaskins, *A review of indirect searches for particle dark matter*, *Contemp. Phys.* **57** (2016) 496 [1604.00014].
- [8] G. Bertone, D. Hooper and J. Silk, *Particle dark matter: Evidence, candidates and constraints*, *Phys. Rept.* **405** (2005) 279 [hep-ph/0404175].
- [9] S. Hawking, *Gravitationally collapsed objects of very low mass*, *Mon. Not. Roy. Astron. Soc.* **152** (1971) 75.
- [10] X. Wang, M. Sasaki and Y.-l. Zhang, *The Dual Primordial Black Hole Formation Scenario*, **2505.09337**.
- [11] E.J. Barroso, L.F. Demétrio, S.D.P. Vitenti and X. Ye, *Primordial black hole formation in a dust bouncing model*, *JCAP* **01** (2025) 052 [2405.00207].

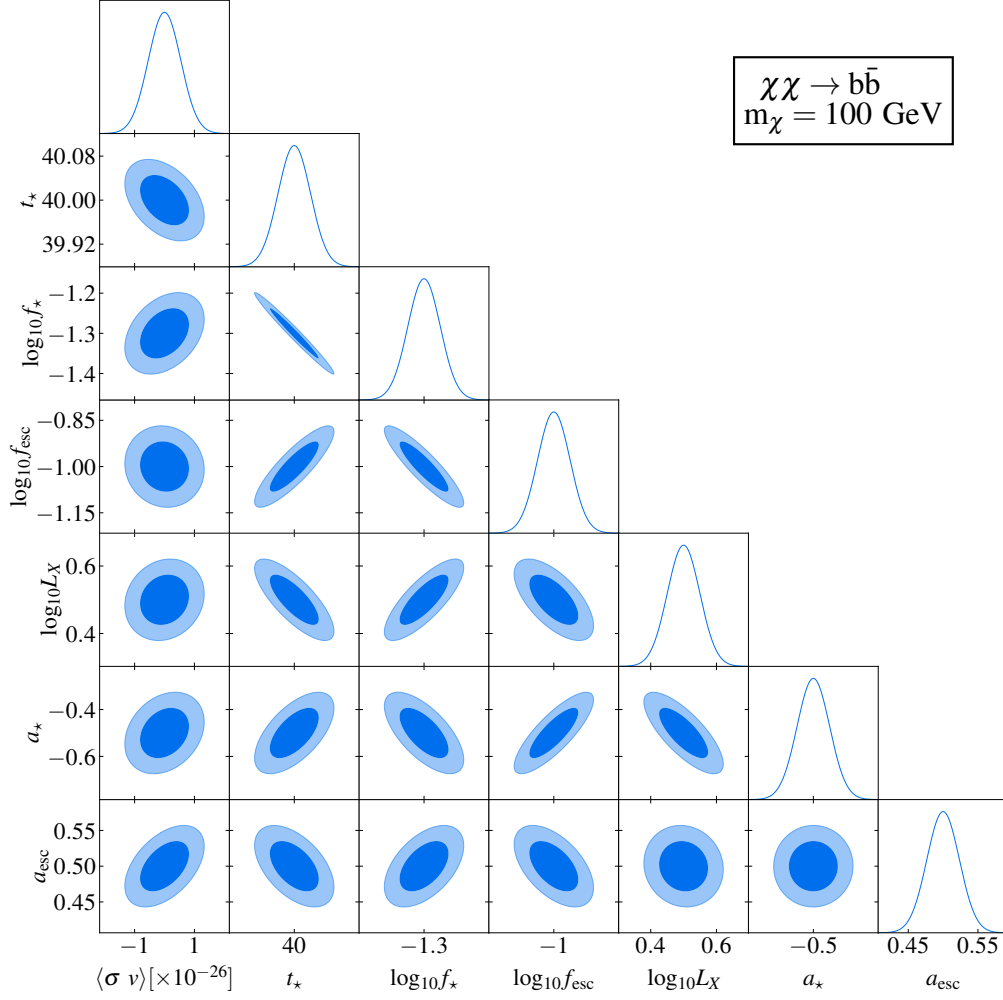


Figure 10. Same as Fig. 9 but for 100 GeV DM particles annihilating into bottom-anti-bottom quark pairs.

- [12] B. Carr and F. Kuhnel, *Primordial black holes as dark matter candidates*, *SciPost Phys. Lect. Notes* **48** (2022) 1 [2110.02821].
- [13] B.J. Carr, K. Kohri, Y. Sendouda and J. Yokoyama, *New cosmological constraints on primordial black holes*, *Phys. Rev. D* **81** (2010) 104019 [0912.5297].
- [14] C. Zhang and X. Zhang, *Gravitational capture of magnetic monopoles by primordial black holes in the early universe*, *JHEP* **10** (2023) 037 [2302.07002].
- [15] C. Zhang and X. Zhang, *Magnetic monopole meets primordial black hole: an extended analysis*, *Eur. Phys. J. C* **84** (2024) 100 [2308.07166].
- [16] N. Jia, S.-S. Bao, C. Zhang, H. Zhang and X. Zhang, *Superradiant dark matter production from primordial black holes: Impact of multiple modes and gravitational wave emission*, 2504.18935.
- [17] V. Mohapatra, *Cosmological bounds on dark matter annihilation using dark ages 21-cm signal*, 2506.20648.
- [18] Y. Shao, T.-Y. Sun, M.-L. Zhao and X. Zhang, *Analytical modeling of the one-dimensional power spectrum of 21-cm forest based on a halo model method*, 2411.17094.
- [19] T.-Y. Sun, Y. Shao, Y. Li, Y. Xu, H. Wang and X. Zhang, *Deep learning-driven likelihood-free parameter inference for 21-cm forest observations*, *Commun. Phys.* **8** (2025) 220 [2407.14298].
- [20] A.J. Nishizawa, P.K. Natwariya and K. Kadota, *Machine learning constraints on dark matter annihilation during the epoch of reionization: A convolutional neural network analysis of the 21-cm signal*, *Phys. Rev. D* **111** (2025) 083546 [2410.04755].
- [21] M.-L. Zhao, S. Wang and X. Zhang, *Prospects for probing dark matter particles and primordial black holes with the Hongmeng mission using the 21 cm global spectrum at cosmic dawn*, *JCAP* **07** (2025) 039 [2412.19257].
- [22] Y. Shao, Y. Xu, Y. Wang, W. Yang, R. Li, X. Zhang et al., *The 21-cm forest as a simultaneous probe of dark matter and cosmic heating history*, *Nature Astron.* **7** (2023) 1116 [2307.04130].

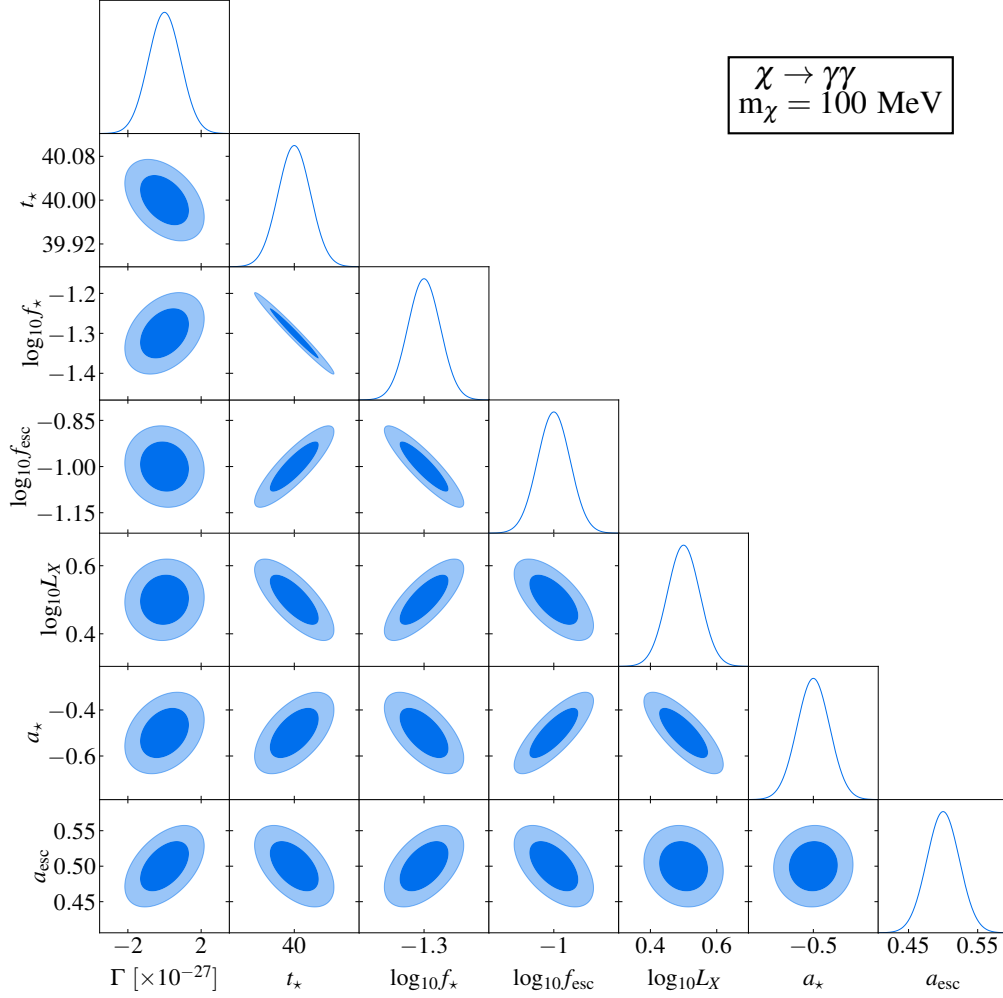


Figure 11. Same as Fig. 9 but for 100 MeV DM particles decaying into photon pairs.

- [23] N. Hiroshima, K. Kohri, T. Sekiguchi and R. Takahashi, *Impacts of new small-scale N -body simulations on dark matter annihilations constrained from cosmological 21-cm line observations*, *Phys. Rev. D* **104** (2021) 083547 [2103.14810].
- [24] A.K. Saha and R. Laha, *Sensitivities on nonspinning and spinning primordial black hole dark matter with global 21-cm troughs*, *Phys. Rev. D* **105** (2022) 103026 [2112.10794].
- [25] J. Cang, Y. Gao and Y.-Z. Ma, *21-cm constraints on spinning primordial black holes*, *JCAP* **03** (2022) 012 [2108.13256].
- [26] O. Mena, S. Palomares-Ruiz, P. Villanueva-Domingo and S.J. Witte, *Constraining the primordial black hole abundance with 21-cm cosmology*, *Phys. Rev. D* **100** (2019) 043540 [1906.07735].
- [27] L. Lopez-Honorez, O. Mena, Á. Moliné, S. Palomares-Ruiz and A.C. Vincent, *The 21 cm signal and the interplay between dark matter annihilations and astrophysical processes*, *JCAP* **08** (2016) 004 [1603.06795].
- [28] C. Xu, W. Qin and T.R. Slatyer, *CMB limits on decaying dark matter beyond the ionization threshold*, *Phys. Rev. D* **110** (2024) 123529 [2408.13305].
- [29] F. Capozzi, R.Z. Ferreira, L. Lopez-Honorez and O. Mena, *CMB and Lyman- α constraints on dark matter decays to photons*, *JCAP* **06** (2023) 060 [2303.07426].
- [30] Z.-X. Zhang, Y.-M. Wang, J. Cang, Z. Zhang, Y. Liu, S.-Y. Li et al., *Dark matter search with CMB: a study of foregrounds*, *JCAP* **10** (2023) 002 [2304.07793].
- [31] S.K. Acharya and R. Khatri, *CMB and BBN constraints on evaporating primordial black holes revisited*, *JCAP* **06** (2020) 018 [2002.00898].
- [32] J. Chluba, A. Ravenni and S.K. Acharya, *Thermalization of large energy release in the early Universe*, *Mon. Not. Roy. Astron. Soc.* **498** (2020) 959 [2005.11325].
- [33] PLANCK collaboration, *Planck 2018 results. VI. Cosmological parameters*, *Astron. Astrophys.* **641** (2020)

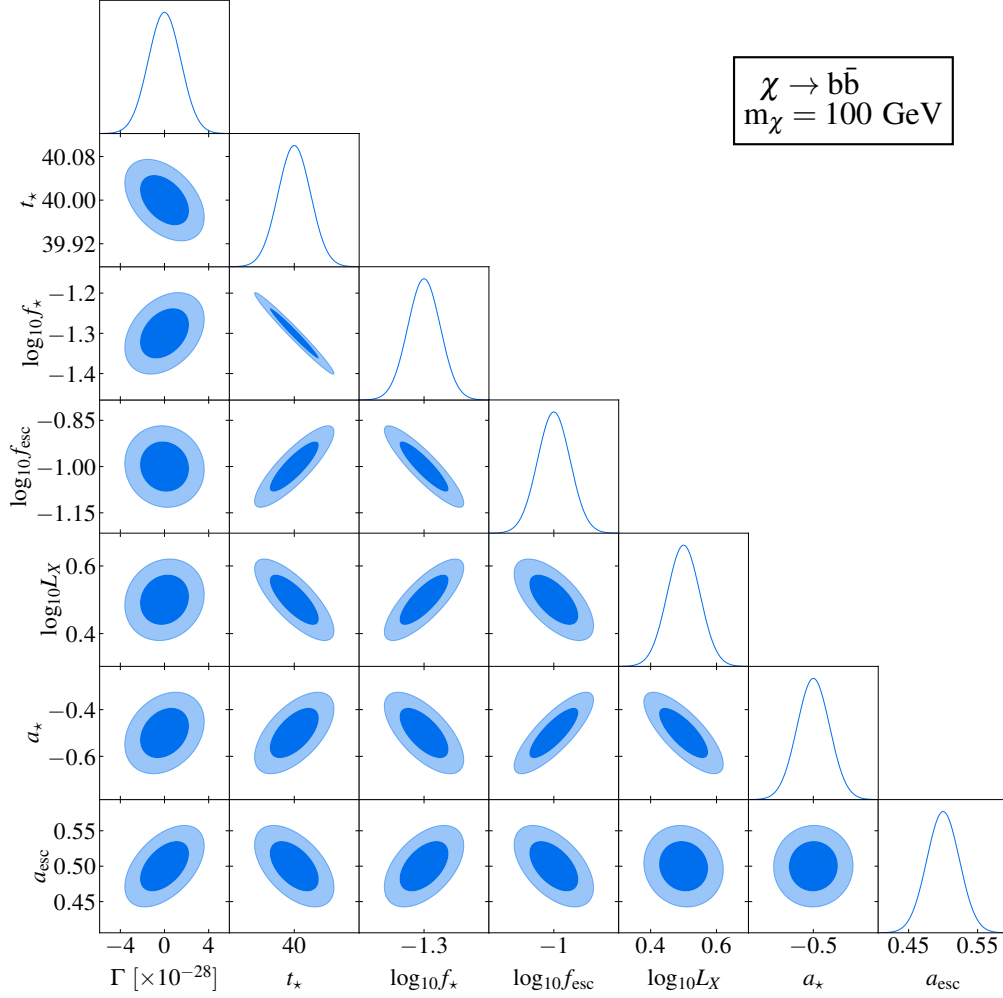


Figure 12. Same as Fig. 9 but for 100 GeV DM particles decaying into bottom-anti-bottom quark pairs.

- A6 [1807.06209].
- [34] S. Clark, B. Dutta, Y. Gao, L.E. Strigari and S. Watson, *Planck Constraint on Relic Primordial Black Holes*, *Phys. Rev. D* **95** (2017) 083006 [1612.07738].
- [35] M. Kawasaki, K. Kohri, T. Moroi and Y. Takaesu, *Revisiting Big-Bang Nucleosynthesis Constraints on Dark-Matter Annihilation*, *Phys. Lett. B* **751** (2015) 246 [1509.03665].
- [36] L. Lopez-Honorez, O. Mena, S. Palomares-Ruiz and A.C. Vincent, *Constraints on dark matter annihilation from CMB observations before Planck*, *JCAP* **07** (2013) 046 [1303.5094].
- [37] T.R. Slatyer, N. Padmanabhan and D.P. Finkbeiner, *CMB Constraints on WIMP Annihilation: Energy Absorption During the Recombination Epoch*, *Phys. Rev. D* **80** (2009) 043526 [0906.1197].
- [38] LHAASO collaboration, *All-sky search for individual Primordial Black Hole bursts with LHAASO*, 2505.24586.
- [39] A.K. Saha, A. Singh, P. Parashari and R. Laha, *Hunting Primordial Black Hole Dark Matter in Lyman- α Forest*, 2409.10617.
- [40] C. Yang, S. Wang, M.-L. Zhao and X. Zhang, *Search for the Hawking radiation of primordial black holes: prospective sensitivity of LHAASO*, *JCAP* **10** (2024) 083 [2408.10897].
- [41] J. Koechler, *X-rays constraints on sub-GeV Dark Matter*, in *TeV Particle Astrophysics 2023*, 9, 2023 [2309.10043].
- [42] F. Calore, A. Dekker, P.D. Serpico and T. Siebert, *Constraints on light decaying dark matter candidates from 16 yr of INTEGRAL/SPI observations*, *Mon. Not. Roy. Astron. Soc.* **520** (2023) 4167 [2209.06299].
- [43] J.W. Foster, Y. Park, B.R. Safdi, Y. Soreq and W.L. Xu, *Search for dark matter lines at the Galactic Center with 14 years of Fermi data*, *Phys. Rev. D* **107** (2023) 103047 [2212.07435].
- [44] N. Bernal, V. Muñoz-Alborno, S. Palomares-Ruiz and P. Villanueva-Domingo, *Current and future neutrino*

- limits on the abundance of primordial black holes, *JCAP* **10** (2022) 068 [2203.14979].
- [45] M. Cirelli, N. Fornengo, B.J. Kavanagh and E. Pinetti, *Integral X-ray constraints on sub-GeV Dark Matter*, *Phys. Rev. D* **103** (2021) 063022 [2007.11493].
- [46] S. Wang, D.-M. Xia, X. Zhang, S. Zhou and Z. Chang, *Constraining primordial black holes as dark matter at JUNO*, *Phys. Rev. D* **103** (2021) 043010 [2010.16053].
- [47] M. Boudaud and M. Cirelli, *Voyager 1 e^\pm Further Constrain Primordial Black Holes as Dark Matter*, *Phys. Rev. Lett.* **122** (2019) 041104 [1807.03075].
- [48] M. Boudaud, T. Lacroix, M. Stref and J. Lavalle, *Robust cosmic-ray constraints on p-wave annihilating MeV dark matter*, *Phys. Rev. D* **99** (2019) 061302 [1810.01680].
- [49] HESS collaboration, *Searches for gamma-ray lines and 'pure WIMP' spectra from Dark Matter annihilations in dwarf galaxies with H.E.S.S.*, *JCAP* **11** (2018) 037 [1810.00995].
- [50] MAGIC collaboration, *Indirect dark matter searches in the dwarf satellite galaxy Ursa Major II with the MAGIC Telescopes*, *JCAP* **03** (2018) 009 [1712.03095].
- [51] VERITAS collaboration, *Dark Matter Constraints from a Joint Analysis of Dwarf Spheroidal Galaxy Observations with VERITAS*, *Phys. Rev. D* **95** (2017) 082001 [1703.04937].
- [52] M. Boudaud, J. Lavalle and P. Salati, *Novel cosmic-ray electron and positron constraints on MeV dark matter particles*, *Phys. Rev. Lett.* **119** (2017) 021103 [1612.07698].
- [53] T. Cohen, K. Murase, N.L. Rodd, B.R. Safdi and Y. Soreq, *γ -ray Constraints on Decaying Dark Matter and Implications for IceCube*, *Phys. Rev. Lett.* **119** (2017) 021102 [1612.05638].
- [54] B.J. Carr, K. Kohri, Y. Sendouda and J. Yokoyama, *Constraints on primordial black holes from the Galactic gamma-ray background*, *Phys. Rev. D* **94** (2016) 044029 [1604.05349].
- [55] FERMI-LAT collaboration, *Searching for Dark Matter Annihilation from Milky Way Dwarf Spheroidal Galaxies with Six Years of Fermi Large Area Telescope Data*, *Phys. Rev. Lett.* **115** (2015) 231301 [1503.02641].
- [56] A. Massari, E. Izaguirre, R. Essig, A. Albert, E. Bloom and G.A. Gómez-Vargas, *Strong Optimized Conservative Fermi-LAT Constraints on Dark Matter Models from the Inclusive Photon Spectrum*, *Phys. Rev. D* **91** (2015) 083539 [1503.07169].
- [57] H.E.S.S. collaboration, *Search for dark matter annihilation signatures in H.E.S.S. observations of Dwarf Spheroidal Galaxies*, *Phys. Rev. D* **90** (2014) 112012 [1410.2589].
- [58] J. Aleksić et al., *Optimized dark matter searches in deep observations of Segue 1 with MAGIC*, *JCAP* **02** (2014) 008 [1312.1535].
- [59] R. Diamanti, L. Lopez-Honorez, O. Mena, S. Palomares-Ruiz and A.C. Vincent, *Constraining Dark Matter Late-Time Energy Injection: Decays and P-Wave Annihilations*, *JCAP* **02** (2014) 017 [1308.2578].
- [60] R. Essig, E. Kuflik, S.D. McDermott, T. Volansky and K.M. Zurek, *Constraining Light Dark Matter with Diffuse X-Ray and Gamma-Ray Observations*, *JHEP* **11** (2013) 193 [1309.4091].
- [61] M. Cirelli, F. Iocco and P. Panci, *Constraints on Dark Matter annihilations from reionization and heating of the intergalactic gas*, *JCAP* **10** (2009) 009 [0907.0719].
- [62] M. Kolopanis, J.C. Pober, D.C. Jacobs and S. McGraw, *New EoR power spectrum limits from MWA Phase II using the delay spectrum method and novel systematic rejection*, *Mon. Not. Roy. Astron. Soc.* **521** (2023) 5120 [2210.10885].
- [63] C.M. Trott et al., *Deep multiredshift limits on Epoch of Reionization 21 cm power spectra from four seasons of Murchison Widefield Array observations*, *Mon. Not. Roy. Astron. Soc.* **493** (2020) 4711 [2002.02575].
- [64] F.G. Mertens et al., *Deeper multi-redshift upper limits on the Epoch of Reionization 21-cm signal power spectrum from LOFAR between $z=8.3$ and $z=10.1$* , **2503.05576**.
- [65] B.K. Gehlot, F.G. Mertens, L.V.E. Koopmans, M.A. Brentjens, S. Zaroubi, B. Ciardi et al., *The first power spectrum limit on the 21-cm signal of neutral hydrogen during the Cosmic Dawn at $z = 20$ -25 from LOFAR*, *mnras* **488** (2019) 4271 [1809.06661].
- [66] Z. Abdurashidova, J.E. Aguirre, P. Alexander, Z.S. Ali, Y. Balfour, A.P. Beardsley et al., *First Results from HERA Phase I: Upper Limits on the Epoch of Reionization 21 cm Power Spectrum*, *apj* **925** (2022) 221 [2108.02263].
- [67] S. Gagnon-Hartman, J. Davies and A. Mesinger, *Detecting galaxy-21-cm cross-correlation during reionization*, **2502.20447**.
- [68] C. Bierlich et al., *A comprehensive guide to the physics and usage of PYTHIA 8.3*, *SciPost Phys. Codeb.* **2022** (2022) 8 [2203.11601].
- [69] M. Cirelli, G. Corcella, A. Hektor, G. Hutsi, M. Kadastik, P. Panci et al., *PPPC 4 DM ID: A Poor Particle Physicist Cookbook for Dark Matter Indirect Detection*, *JCAP* **03** (2011) 051 [1012.4515].
- [70] H. Liu, G.W. Ridgway and T.R. Slatyer, *Code package for calculating modified cosmic ionization and thermal histories with dark matter and other exotic energy injections*, *Phys. Rev. D* **101** (2020) 023530 [1904.09296].
- [71] T.R. Slatyer, *Indirect Dark Matter Signatures in the Cosmic Dark Ages II. Ionization, Heating and Photon Production from Arbitrary Energy Injections*, *Phys. Rev. D* **93** (2016) 023521 [1506.03812].
- [72] T.R. Slatyer, *Indirect dark matter signatures in the cosmic dark ages. I. Generalizing the bound on s-wave dark matter annihilation from Planck results*, *Phys. Rev. D* **93** (2016) 023527 [1506.03811].
- [73] T.R. Slatyer, *Energy Injection And Absorption In The Cosmic Dark Ages*, *Phys. Rev. D* **87** (2013) 123513 [1211.0283].
- [74] J. Auffinger and A. Arbey, *BlackHawk: A tool for computing Black Hole evaporation*, *PoS TOOLS2020* (2021) 024 [2012.12902].
- [75] G. Facchinetti, L. Lopez-Honorez, Y. Qin and A. Mesinger, *21cm signal sensitivity to dark matter decay*, *JCAP* **01** (2024) 005 [2308.16656].
- [76] J.R. Pritchard and A. Loeb, *21-cm cosmology*, *Rept. Prog. Phys.* **75** (2012) 086901 [1109.6012].
- [77] S. Furlanetto, S.P. Oh and F. Briggs, *Cosmology at Low Frequencies: The 21 cm Transition and the High-Redshift Universe*, *Phys. Rept.* **433** (2006) 181 [astro-ph/0608032].
- [78] A. Mesinger, S. Furlanetto and R. Cen, *21cmFAST: A Fast, Semi-Numerical Simulation of the High-Redshift*

- 21-cm Signal*, *Mon. Not. Roy. Astron. Soc.* **411** (2011) 955 [1003.3878].
- [79] C.A. Mason, J.B. Muñoz, B. Greig, A. Mesinger and J. Park, *21cmfish: Fisher-matrix framework for fast parameter forecasts from the cosmic 21-cm signal*, *Mon. Not. Roy. Astron. Soc.* **524** (2023) 4711 [2212.09797].
- [80] J.C. Pober, A.R. Parsons, D.R. DeBoer, P. McDonald, M. McQuinn, J.E. Aguirre et al., *The Baryon Acoustic Oscillation Broadband and Broad-beam Array: Design Overview and Sensitivity Forecasts*, *Astron. J.* **145** (2013) 65 [1210.2413].
- [81] O. Zahn, A. Mesinger, M. McQuinn, H. Trac, R. Cen and L.E. Hernquist, *Comparison Of Reionization Models: Radiative Transfer Simulations And Approximate, Semi-Numeric Models*, *Mon. Not. Roy. Astron. Soc.* **414** (2011) 727 [1003.3455].
- [82] R. Braun, A. Bonaldi, T. Bourke, E. Keane and J. Wagg, *Anticipated Performance of the Square Kilometre Array – Phase 1 (SKA1)*, **1912.12699**.
- [83] M. Fréchet, *Sur l'extension de certaines évaluations statistiques au cas de petits échantillons*, *Revue de l'Institut International de Statistique* (1943) 182.
- [84] A. Mesinger, A. Ewall-Wice and J. Hewitt, *Reionization and beyond: detecting the peaks of the cosmological 21 cm signal*, *Mon. Not. Roy. Astron. Soc.* **439** (2014) 3262 [1310.0465].
- [85] M. Chhabra and S. Bharadwaj, *Probing the HI distribution at small scales using 21-cm Intensity Mapping at large scales*, **2508.19126**.
- [86] S.S. Gill, S. Bharadwaj, K.M.A. Elahi, S.K. Sethi and A.K. Patwa, *The EoR 21-cm Bispectrum at $z = 8.2$ from MWA data I: Foregrounds and preliminary upper limits*, **2507.04964**.
- [87] L. Noble, M. Kamran, S. Majumdar, C.S. Murmu, R. Ghara, G. Mellema et al., *Impact of the Epoch of Reionization sources on the 21-cm bispectrum*, *JCAP* **10** (2024) 003 [2406.03118].
- [88] K. Diao and Y. Mao, *Multi-fidelity emulator for large-scale 21 cm lightcone images: a few-shot transfer learning approach with generative adversarial network*, **2502.04246**.
- [89] H. Shimabukuro, Y. Xu and Y. Shao, *Analyzing the 21cm forest with Wavelet Scattering Transform: Insight into non-Gaussian features of the 21cm forest*, **2504.14656**.
- [90] X. Zhao, Y. Mao, S. Zuo and B.D. Wandelt, *Simulation-based Inference of Reionization Parameters from 3D Tomographic 21 cm Light-cone Images. II. Application of Solid Harmonic Wavelet Scattering Transform*, *Astrophys. J.* **973** (2024) 41 [2310.17602].
- [91] K. Diao, Z. Chen, X. Chen and Y. Mao, *Reionization Parameter Inference from 3D Minkowski Functionals of the 21 cm Signals*, *Astrophys. J.* **974** (2024) 141 [2406.20058].
- [92] Z. Li, Z. Cai, X. Wang, Z. Li, A. Dekel, K.C. Sarkar et al., *A 13-Billion-Year View of Galaxy Growth: Metallicity Gradient Evolution from the Local Universe to $z = 9$ with JWST and Archival Surveys*, *arXiv e-prints* (2025) arXiv:2506.12129 [2506.12129].